

Dynamical mean field theory algorithm and experiment on quantum computers

I. Rungger,^{1,*} N. Fitzpatrick,² H. Chen,^{3,4} C. H. Alderete,^{5,6} H. Apel,^{2,7} A. Cowtan,² A. Patterson,⁷ D. Muñoz Ramo,² Y. Zhu,⁵ N. H. Nguyen,⁵ E. Grant,^{3,4} S. Chretien,¹ L. Wossnig,^{3,4} N. M. Linke,⁵ and R. Duncan^{2,8}

¹*National Physical Laboratory, Teddington, TW11 0LW, United Kingdom*

²*Cambridge Quantum Computing Ltd, 9a Bridge Street, Cambridge, United Kingdom*

³*Rahko Ltd., Finsbury Park, N4 3JP, United Kingdom*

⁴*Dept. of Computer Science, University College London, Gower Street, London, WC1E 6BT, United Kingdom*

⁵*Joint Quantum Institute, Department of Physics, University of Maryland, College Park, MD 20742, USA*

⁶*Instituto Nacional de Astrofísica, Óptica y Electrónica, Calle Luis Enrique Erro No. 1, Sta. Ma. Tonantzintla, Pue. CP 72840, Mexico*

⁷*Dept. of Physics and Astronomy, University College London,*

Gower Street, London, WC1E 6BT, United Kingdom

⁸*Department of Computer and Information Sciences, University of Strathclyde, 26 Richmond Street, Glasgow, United Kingdom*

The developments of quantum computing algorithms and experiments for atomic scale simulations have largely focused on quantum chemistry for molecules, while their application in condensed matter systems is scarcely explored. Here we present a quantum algorithm to perform dynamical mean field theory (DMFT) calculations for condensed matter systems on currently available quantum computers, and demonstrate it on two quantum hardware platforms. DMFT is required to properly describe the large class of materials with strongly correlated electrons. The computationally challenging part arises from solving the effective problem of an interacting impurity coupled to a bath, which scales exponentially with system size on conventional computers. An exponential speedup is expected on quantum computers, but the algorithms proposed so far are based on real time evolution of the wavefunction, which requires very low noise levels in the quantum hardware. Here we propose an alternative approach, which uses the variational quantum eigensolver (VQE) method for ground and excited states to obtain the needed quantities as part of an exact diagonalization impurity solver. We present the algorithm for a two site DMFT system, which we benchmark using simulations on conventional computers as well as experiments on superconducting and trapped ion qubits, demonstrating that this method is suitable for running DMFT calculations on currently available quantum hardware.

I. INTRODUCTION

Computers have an integral role in the design process of new materials and chemicals, predicting and explaining the behavior of the systems in question¹⁻⁴. Such simulations are mostly based on density functional theory (DFT) due to its low computational cost and simplicity of use¹. DFT allows for the computation of important properties, such as atomic structures, chemical reaction rates and the electronic structure of solids. However, in many instances DFT fails to correctly predict the observed behavior⁵, for example Mott insulator transitions⁶ or the binding of oxygen to haemoglobin^{7,8}. The reason is that DFT treats the quantum mechanical interactions between electrons within an effective mean field approximation, which becomes invalid when the electrons are strongly correlated with each other. A number of corrections have been developed to overcome the limitations of DFT⁹, such as hybrid functionals¹⁰, self-interaction corrections¹¹, or the GW approximation¹². For solid state systems, where local electron-electron correlations are strong, the dynamical mean field theory (DMFT) is the state-of-the-art correction to DFT¹³⁻¹⁵. In DMFT one separates out the strongly interacting local orbitals as an effective impurity from the remaining part of the system,

which is treated as an effective bath together with the orbitals of neighboring atoms. Example cases where DMFT overcomes the failures of DFT include Mott insulators⁶ and superconducting systems¹⁶, molecules on surfaces exhibiting Kondo behavior¹⁷, and also extend to biochemical systems¹⁸ and metalloproteins such as haemoglobin⁸. Metalloproteins play an important role within the pharmaceutical sector, such as the therapeutic application of hemocyanins¹⁹, a very promising class of anti-cancer therapeutics.

However, the high computational cost required for accurate solutions limits DMFT to small systems on the currently available conventional computers. Quantum computers can in principle solve correlated electronic structure problems in polynomial time²⁰⁻²² using algorithms such as phase estimation²³. While large-scale quantum computers are still out of reach, small, so called noisy intermediate scale quantum computers²⁴ have recently become available, and have sparked a growing interest in demonstrating applications on existing devices. In particular, quantum-classical hybrid algorithms, such as the variational quantum eigensolver (VQE)²⁵, have been shown to enable simulations for small molecules and simplified model Hamiltonians^{26,27}, perform learning tasks²⁸⁻³¹ or even algebraic operations³². However,

due to the noise levels and limited size of current quantum computers simulations of large molecules or materials systems are still out of reach. Embedding methods such as DMFT may overcome this problem, since here the computationally demanding part of the calculation is performed only on a smaller subsystem. A recent proposal demonstrates that such methods can also be formulated using quantum algorithms^{33,34}. In these approaches the computationally intensive part of the DMFT calculation is executed on a quantum device, while the remaining part is done classically. This hybrid approach has been simulated on a conventional computer for a small prototype system of 2 sites³⁵ within the framework of 2-site DMFT³⁶.

To date no hybrid quantum-classical algorithm that solves the DMFT formalism has been implemented on an actual quantum device, because prior methods have been unable to deal with the high levels of noise in these machines. Here we expand upon prior work by introducing a VQE-based quantum-classical hybrid algorithm, which allows us to run the 2-site DMFT system on a quantum device. The quantum computer solves the effective quantum impurity problem, which in the DMFT loop is self-consistently determined via a feedback between the quantum and classical computation. We use VQE to implement an exact diagonalization solver³⁷⁻³⁹, and demonstrate that our algorithm can tackle the electronic structure problem of correlated materials using quantum devices available today. This method can be scaled to larger system sizes as the available number of qubits increases, where its efficiency relies on the scalability of the underlying VQE, which is an active area of research^{40,41}. With that, we believe our method will allow many open questions in quantum materials to be resolved once a intermediate scale quantum computer with around 100 qubits becomes available.

II. QUANTUM ALGORITHM

A. Dynamical mean field theory

Within DMFT the extended lattice model is mapped to an effective Anderson impurity problem with Hamiltonian operator \hat{H} , where the interacting region is coupled to an infinitely extended bath¹³⁻¹⁵. Here we use the exact diagonalization (ED) approximation as the impurity solver, where a finite number of effective sites is used to represent the bath³⁷⁻³⁹. To map this ED Hamiltonian to a quantum computer we perform a Jordan-Wigner transform⁴². As a matter of notation we label quantities associated with the N_{imp} impurity spin orbitals with Greek subscripts $\alpha, \beta, \gamma, \delta$. The spin orbital index is a collective index that includes both orbital and spin degrees of freedom, so that for example $\alpha = 1$ represents the spin orbital $(1, \uparrow)$, where the first integer indicates the site index and the arrow the spin direction, $\alpha = 2$ represents $(1, \downarrow)$, $\alpha = 3$ represents $(2, \uparrow)$, and so on, un-

til the index $\alpha = 2N_{\text{imp}}$ represents $(N_{\text{imp}}, \downarrow)$. The spin orbitals associated with the N_{b} bath orbitals are labeled with i, j subscripts, and the ones associated with any of the $N_{\text{imp}} + N_{\text{b}}$ orbitals with n and m subscripts. Within ED the impurity Hamiltonian is usually written as^{33,39,43}

$$\hat{H} = \hat{H}_{\text{imp}} + \hat{H}_{\text{bath}} + \hat{H}_{\text{mix}}, \quad (1)$$

$$\hat{H}_{\text{imp}} = \sum_{\alpha} (\epsilon_{\alpha} - \mu) \hat{\sigma}_{\alpha}^{-} \hat{\sigma}_{\alpha}^{+} + \sum_{\alpha\beta\gamma\delta} U_{\alpha\beta\gamma\delta} \hat{\sigma}_{\alpha}^{-} \hat{\sigma}_{\beta}^{-} \hat{\sigma}_{\gamma}^{+} \hat{\sigma}_{\delta}^{+}, \quad (2)$$

$$\hat{H}_{\text{mix}} = \sum_{\alpha i} (V_{\alpha i} \hat{\sigma}_{\alpha}^{-} \hat{\sigma}_i^{+} + V_{\alpha i}^{*} \hat{\sigma}_i^{-} \hat{\sigma}_{\alpha}^{+}), \quad (3)$$

$$\hat{H}_{\text{bath}} = \sum_i \epsilon_i \hat{\sigma}_i^{-} \hat{\sigma}_i^{+}, \quad (4)$$

where μ is the chemical potential, ϵ_{α} are the internal onsite energies of the impurity, $U_{\alpha\beta\gamma\delta}$ are the electron interaction energies, $V_{\alpha i}$ are the hopping matrix elements between the impurity and the bath, and the ϵ_i denote the onsite energies of the bath orbitals. Here we have introduced a modified form of the Pauli ladder operators that takes into account the fermionic nature of the electrons

$$\hat{\sigma}_{\alpha}^{\pm} = \left(\prod_{\beta=1}^{\alpha-1} \hat{\sigma}_{\beta}^z \right) \frac{1}{2} (\hat{\sigma}_{\alpha}^x \pm i \hat{\sigma}_{\alpha}^y), \quad (5)$$

$$\hat{\sigma}_i^{\pm} = \left(\prod_{\beta=1}^{N_{\text{imp}}} \hat{\sigma}_{\beta}^z \right) \left(\prod_{j=1}^{i-1} \hat{\sigma}_j^z \right) \frac{1}{2} (\hat{\sigma}_i^x \pm i \hat{\sigma}_i^y). \quad (6)$$

With this definition $\hat{\sigma}_{\alpha}^{-}$ ($\hat{\sigma}_{\alpha}^{+}$) creates (destroys) an electron on spin orbital α . The total number of qubits to represent \hat{H} is $2(N_{\text{imp}} + N_{\text{b}})$.

We can calculate all the energy eigenvalues of \hat{H} , $E_{N,n}$, and the corresponding eigenvectors, $|\psi_{N,n}\rangle$. Here the integer N denotes the number of electrons of the state, and the integer n goes from 0 to the number of eigenstates with N electrons minus one, M_N . We order the states by increasing energy, so that $|\psi_{N,0}\rangle$ is the ground state for N electrons, $|\psi_{N,1}\rangle$ is the first excited state and so on, until the highest excited state for N electrons $|\psi_{N,M_N}\rangle$. We denote as N_0 the number of electrons of the overall ground state, and label the ground state (GS) as $|\psi_0\rangle = |\psi_{N_0,0}\rangle$, with $E_0 = E_{N_0,0}$.

Within DMFT the central quantities are the local retarded Green's functions (GFs) of the original lattice model, $G_{\text{lat}}(\omega)$, and of the impurity problem, $G(\omega)$. Here ω is the real or imaginary energy. The central condition of DMFT is that locally on the interacting site the impurity problem is equivalent to the lattice problem, which leads to the condition that $G_{\text{lat}}(\omega) = G(\omega)$. This condition can only be exactly satisfied if an infinite number of bath sites is used. For a finite number of bath sites in ED one typically aims at effectively minimizing the difference between $G_{\text{lat}}(\omega)$ and $G(\omega)$. In practice one starts from some initial guess for impurity Hamiltonian parameters ϵ_{α} , ϵ_i and $V_{\alpha i}$, and uses them to calculate $G(\omega)$. From

these quantities and the original lattice Hamiltonian one obtains $G_{\text{lat}}(\omega)$. At this stage the one updates ϵ_α , ϵ_i and $V_{\alpha i}$ to effectively aim to minimize the difference between $G(\omega)$ and $G_{\text{lat}}(\omega)$. One then iterates this procedure until ϵ_α , ϵ_i and $V_{\alpha i}$ reach self-consistency. This process is denoted as the DMFT loop (Fig. 1)³⁹.

We now assume that the local GF off-diagonal terms are small enough, so that they can be neglected. Note that we use this assumption only to simplify the notation, and one can equivalently formulate the algorithm also for dense GFs. We use the Lehman representation of the diagonal elements of the zero temperature impurity GF, $G_\alpha(\omega)$, which are generally given by

$$G_\alpha(\omega) = \sum_{n=0}^{M_{N_0-1}} \frac{\lambda_{h,\alpha,n}}{\omega + i\delta - \omega_{h,n}} + \sum_{n=0}^{M_{N_0+1}} \frac{\lambda_{p,\alpha,n}}{\omega + i\delta - \omega_{p,n}}, \quad (7)$$

where the first summation goes over all states with one electron removed from the ground state (hole states), while the second summation goes over all states with one electron added to it (particle states). Here δ is an infinitesimally small positive number, and

$$\omega_{h,n} = E_0 - E_{N_0-1,n}, \quad (8)$$

$$\lambda_{h,\alpha,n} = \left| \left\langle \psi_{N_0-1,n} \left| \left(\prod_{\beta=1}^{\alpha-1} \hat{\sigma}_\beta^z \right) \hat{\sigma}_\alpha^x \right| \psi_0 \right\rangle \right|^2, \quad (9)$$

$$\omega_{p,n} = E_{N_0+1,n} - E_0, \quad (10)$$

$$\lambda_{p,\alpha,n} = \left| \left\langle \psi_{N_0+1,n} \left| \left(\prod_{\beta=1}^{\alpha-1} \hat{\sigma}_\beta^z \right) \hat{\sigma}_\alpha^x \right| \psi_0 \right\rangle \right|^2. \quad (11)$$

Note that in Eqs. (9) and (11) we use the fact that the number of electrons of the states in the brackets differs by one. For increasing $N_{\text{imp}} + N_{\text{b}}$ the total number of excited states $M_{N_0 \pm 1}$ becomes exponentially large. However, in practical calculations one typically needs only the low energy excitations up to a specified energy cutoff, which are needed to represent $G_\alpha(\omega)$ in the desired energy range around 0.

We can equivalently write $G_\alpha(\omega)$ as

$$G_\alpha(\omega) = \frac{1}{\omega + i\delta + \mu - \Delta_\alpha(\omega) - \Sigma_\alpha(\omega)}, \quad (12)$$

where the so-called hybridization function is given by

$$\Delta_\alpha(\omega) = \sum_i \frac{|V_{\alpha i}|^2}{\omega + i\delta - \epsilon_i}, \quad (13)$$

and we have introduced the many-body self-energy, $\Sigma_\alpha(\omega)$, which includes all the modification to the non-interacting Green's function, $G_{0,\alpha}(\omega) = \frac{1}{\omega + i\delta + \mu - \Delta_\alpha(\omega)}$, induced by the interaction term proportional to U in the Hamiltonian. It can be written in general form as $\Sigma_\alpha(\omega) = G_{0,\alpha}^{-1}(\omega) - G_\alpha^{-1}(\omega)$. In our quantum algorithm

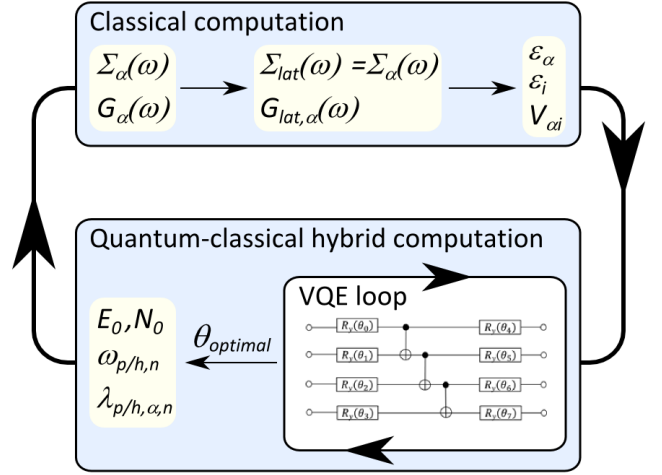


FIG. 1. Schematic of the ED DMFT loop: we start by choosing initial values of the impurity Hamiltonian parameters $\{\epsilon_\alpha, \epsilon_i, V_{\alpha i}\}$, which we then use as input to the quantum computing part of the loop; here we use a VQE quantum circuit to obtain as output all the $\{\omega_{p/h,n}, \lambda_{p/h,\alpha,n}\}$. These are then passed as input to the classical computing part of the loop, where the GFs and self-energies are computed to obtain updated parameters $\{\epsilon_\alpha, \epsilon_i, V_{\alpha i}\}$. These are then again passed to the quantum computing part of the loop, and the process is iterated until the $\{\epsilon_\alpha, \epsilon_i, V_{\alpha i}\}$ are equal within a specified tolerance between subsequent iterations. Once this DMFT self-consistency is achieved, one can use the obtained self-consistent impurity Hamiltonian parameters to calculate the electronic structure of the system.

we determine $G_\alpha(\omega)$ with calculations on a quantum computer, which means that we evaluate the quantities in Eqs. (8-11) on a quantum device. The remaining computations of the DMFT calculation are performed on a classical computer (Fig. 1).

B. Quantum Circuits

In principle $\omega_{p/h,n}$ and $\lambda_{p/h,\alpha,n}$ can be obtained by performing a Fourier transform of the real-time GF^{33,35}. However, the error induced by the finite time steps used to evaluate the real-time GF grows for larger interaction strengths, and therefore the method requires very small time steps. On the currently available quantum computers this leads to noise levels in the results that do not allow for accurate computations of these quantities. We therefore propose to calculate $\omega_{p/h,n}$ and $\lambda_{p/h,\alpha,n}$ via total energy calculations based on a variational quantum eigensolver (VQE), which is generally more resilient to noise^{25,26,44,45}. This approach has also been suggested in a recent article for general Green's function based calculations⁴⁶. In the following we only present the method to calculate $\omega_{p,n}$ and $\lambda_{p,\alpha,n}$, since the procedure to obtain $\omega_{h,n}$ and $\lambda_{h,\alpha,n}$ is analogous.

We represent a general eigenstate of \hat{H} on the quantum

computer by

$$|\psi_{N,n}\rangle = \hat{U}_{N,n} |0\rangle, \quad (14)$$

where $\hat{U}_{N,n}$ is a unitary operator. We typically use a hardware efficient ansatz to apply $\hat{U}_{N,n}$ to the state $|0\rangle$ in our quantum circuit⁴⁷. Note that for the common case where the parameters in \hat{H} are real, all the expansion coefficients of the $|\psi_{N,n}\rangle$ can be made real as well, so that $\hat{U}_{N,n}$ can be restricted to real operators. We therefore typically do not need to include any R_x rotations in our ansatz, since these would only be required if the coefficients have a complex component, and instead use only R_y rotations.

We first prepare the state $|\psi_0\rangle$ by varying the parameters of the ansatz quantum circuit to minimize the total energy and obtain E_0 and with it N_0 . To then calculate the spectrum of the $N_0 + 1$ and $N_0 - 1$ electron states we use a modified Hamiltonian,

$$\hat{H} = \hat{H} + \beta \left(\hat{N} - N_{\text{target}} \right)^2. \quad (15)$$

Here $\hat{N} = \sum_{\alpha} \hat{n}_{\alpha} + \sum_i \hat{n}_i$ is the total number operator, where $\hat{n}_{\alpha(i)} = \hat{\sigma}_{\alpha(i)}^{-} \hat{\sigma}_{\alpha(i)}^{+}$ is the number operator on spin orbital $\alpha(i)$. In \hat{H} a penalty term proportional to a real parameter β is added to enforce the target electron number N_{target} ^{48,49}, in our case $N_{\text{target}} = N_0 \pm 1$. To calculate the ground state and excited states of \hat{H} one can then use a number of methods^{50,51}. Here we use the method proposed in Ref.⁵¹, which finds the excited states by penalizing the overlap of the higher energy eigenstates with the previously found lower energy eigenstates.

With this method Eqs. (8-11) can be evaluated. To calculate $\lambda_{p,\alpha,n}$ without increasing the number of qubits we combine Eqs. (11) and (14) to

$$\lambda_{p,\alpha,n} = \left| \langle 0 | U_{N_0+1,\alpha}^{\dagger} \hat{\sigma}_{\alpha}^x U_{N_0,0} | 0 \rangle \right|^2. \quad (16)$$

We therefore obtain $\lambda_{p,\alpha,n}$ on a quantum device by evaluating the quantum circuit corresponding to $U_{N_0+1,\alpha}^{\dagger} \hat{\sigma}_{\alpha}^x U_{N_0,0}$ and measuring the probability of finding the $|0\rangle$ state at the end.

C. Regularization

With the quantities in Eqs. (8-11) calculated on a quantum computer one can in principle perform the full DMFT loop in Fig. 1. However, the small deviations of the calculated quantities from the exact values lead to the presence of unphysical poles in $\Sigma(\omega)$, and hence the DMFT loop does usually not converge. These unphysical divergences are found at the energies where $G_0(\omega)$ is 0, since $\Sigma(\omega) = G_0^{-1}(\omega) - G^{-1}(\omega)$. The exact interacting $G(\omega)$ has divergences at the same energies, which exactly cancel out the divergences due to $G_0(\omega)$. For the

approximate $G(\omega)$ calculated with the quantum circuit the cancellation is only partial. We therefore need to add a regularization to the calculated quantities, which are modified in order to restore the exact cancellation of the divergences of $G_0(\omega)$. The set of energies, at which $G_0(\omega) = 0$, corresponds to the one where $\Delta(\omega)$ in Eq. (13) has a pole, and is therefore equal to the set $\{\epsilon_i\}$. Cancellation of the divergences in $\Sigma(\omega)$ therefore requires that $G(\epsilon_i) = 0$ and $dG(\omega)/d\omega = dG_0(\omega)/d\omega|_{\omega=\epsilon_i}$ for all ϵ_i . Together with Eq. (7) we then obtain the constraints

$$\sum_{n=0}^{M_{N_0-1}} \frac{\lambda_{h,\alpha,n}}{\epsilon_i - \omega_{h,\alpha}} + \sum_{n=0}^{M_{N_0+1}} \frac{\lambda_{p,\alpha,n}}{\epsilon_i - \omega_{p,\alpha}} = 0. \quad (17)$$

$$\sum_{n=0}^{M_{N_0-1}} \frac{\lambda_{h,\alpha,n}}{(\epsilon_i - \omega_{h,\alpha})^2} + \sum_{n=0}^{M_{N_0+1}} \frac{\lambda_{p,\alpha,n}}{(\epsilon_i - \omega_{p,\alpha})^2} = \frac{1}{V_i^2}. \quad (18)$$

In principle one can therefore evaluate all quantities on a quantum computer, and then perform a constrained minimization procedure, where all $\lambda_{p/h,\alpha,n}$ and $\omega_{p/h,n}$ are modified by as little as possible to satisfy the constraints above. This can be a challenging task for increasing system size. We therefore propose to perform the constrained minimization only on the $\lambda_{p,a,\alpha,n}$, while fixing the $\omega_{p/h,n}$. The reason is that in general we expect that the $\omega_{p/h,n}$ are calculated more accurately than the $\lambda_{p/h,\alpha,n}$, since the quantum circuit for the $\lambda_{p/h,\alpha,n}$ is longer. Since Eqs. (17) and (18) are linear in the $\lambda_{p/h,\alpha,n}$, the constrained minimization is less demanding even for larger system sizes. Alternatively, we can also impose these constraints simply by calculating a few of the $\lambda_{p/h,\alpha,n}$ using these equations rather than on the quantum computer. Overall the regularization is therefore scalable to large system sizes.

III. 2-SITE DMFT SIMULATIONS AND EXPERIMENTS

A. 2-site DMFT model

As proof of concept system we consider the 2-site DMFT model presented in Ref.^{35,36}, which solves the single-band Hubbard model on the Bethe lattice with infinite connectivity using exact diagonalization of a two site impurity problem with one interacting and one bath site. Here we only present the parts required to perform the quantum computing DMFT calculations, for a detailed description of the model we refer to Ref.³⁶. For this system \hat{H} from Eq. (1) becomes

$$\hat{H} = \frac{U}{4} \hat{\sigma}_1^z \hat{\sigma}_3^z + \left(\frac{\mu}{2} - \frac{U}{4} \right) (\hat{\sigma}_1^z + \hat{\sigma}_3^z) - \epsilon_2 (\hat{\sigma}_2^z + \hat{\sigma}_4^z) + \frac{V}{2} (\hat{\sigma}_1^x \hat{\sigma}_2^x + \hat{\sigma}_1^y \hat{\sigma}_2^y + \hat{\sigma}_3^x \hat{\sigma}_4^x + \hat{\sigma}_3^y \hat{\sigma}_4^y). \quad (19)$$

Note that here we use a slightly modified mapping of indices between spin orbitals and qubits from what used in

Eq. (1) in order to slightly reduce the number of resulting Pauli operators: qubit 1 (2) represents \uparrow electrons on site 1 (2), while qubit 3 (4) represents a \downarrow electron on site 1 (2).

In 2-site DMFT there are only two bath parameters that can be optimized in the DMFT self-consistent loop, ϵ_2 and $V = V_{12}$. The conditions for DMFT self-consistency derived in Ref.³⁶ are

$$n_{\text{imp}} = n_{\text{lat}}, \quad (20)$$

$$V^2 = z, \quad (21)$$

where we have implicitly set the unit of energy equal to the unscaled hopping of the Bethe lattice. Here $n_{\text{imp}} = \int_{-\infty}^0 \text{DOS}_{\text{imp}}(\omega) d\omega$ is the occupation of the impurity, with the impurity density of states (DOS) given by $\text{DOS}_{\text{imp}}(\omega) = -\frac{2}{\pi} \text{Im}[G(\omega + i\delta)]$, and $n_{\text{lat}} = \int_{-\infty}^0 \text{DOS}_{\text{lat}}(\omega) d\omega$ is the occupation of one Bethe lattice site in the periodic system, with the DOS of the Bethe lattice $\text{DOS}_{\text{lat}}(\omega) = 2\rho_0[\omega + i\delta + \mu - \Sigma(\omega)]$, and $\rho_0(x) = (1/2\pi)\sqrt{4-x^2}$. In Eq. (21) We have introduced the quasi-particle weight z , also known as the wave-function re-normalization factor, defined as $z = 1/\left(1 - \frac{d\text{Re}[\Sigma(\omega)]}{d\omega}\Big|_{\omega=0}\right) = 1/\left(1 - \frac{\text{Im}[\Sigma(i\delta)]}{\delta}\right)$. 2-site DMFT self-consistency therefore requires updating ϵ_2 and V until Eqs. (20) and (21) are satisfied within a desired tolerance.

B. Quantum computing implementation

For our simulations we consider the particle-hole (ph) symmetric case, where $\mu = U/2$ and $\epsilon_2 = 0$, so that the condition in Eq. (20) is automatically satisfied, and we only have to update V until $V^2 - z < \eta$ to satisfy the condition in Eq. (21), with η a small finite tolerance³⁵. Note however that our scheme is generally applicable also away from ph symmetry. At each step of this iterative procedure we have a fixed pair of U and V as input to the quantum computation, which then provides as output the corresponding values for $\omega_{p/h,n}$ and $\lambda_{p/h,\alpha,n}$. At ph symmetry we have $\omega_{h,n} = -\omega_{p,n}$ and $\lambda_{h,\alpha,n} = \lambda_{p,\alpha,n}$, so that we need to perform the computations only for the particle contributions. To demonstrate the applicability of our DMFT method on current quantum hardware we therefore need to show that these quantities computed in an experiment deviate only little from the exact analytical numbers, which we do in the remaining part of the manuscript.

We independently use both the approach of circuit reduction (CR) and of the additional penalty term (PT) in the Hamiltonian (Eq. (15)) to obtain energies at the required number of electrons (see Sec. II B). Within the PT approach we use the full 4-qubit Hamiltonian in Eq. (19) to calculate E_0 , N_0 and $U_{N_0,0}$, and then the states for $N_0 + 1$ electrons to obtain all quantities in Eqs. (8-11). We use the circuit based on the hardware efficient approach for real Hamiltonians, with two layers of rotation

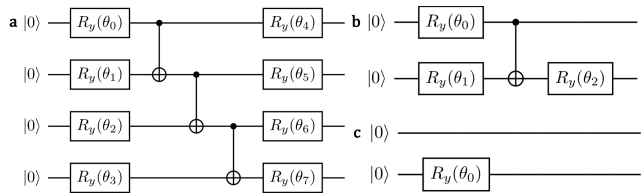


FIG. 2. a) Quantum circuit for the 4-qubit DMFT calculation based on the perturbed Hamiltonian (PT) approach; b) and c) 2-qubit circuits used in the CR approach: b) circuit for the 2 electron singlet ground state calculation; c) circuit for the 1 and 3 electron spectrum calculations. Since the expansion coefficients of our states are real, we only use R_y rotations.

gates and one layer of entangling gates, giving a total of 8 angles to be optimized (Fig. 2a).

For the CR approach we design a separate reduced circuit for each different N and total spin, with a corresponding mapping to a reduced Hamiltonian. In this case no penalty term is needed, and one can just run normal VQE on the individual circuits to determine the ground state, and subsequently calculate the excited states for the $N_0 \pm 1$ circuits. In this case the circuits can be reduced to 2 qubits for all N , which then also allows the calculation of the overlap terms with Eq. (11). For one and three electrons the resulting effective 2-qubit Hamiltonian is identical due to particle-hole symmetry, and is $\hat{H} = \frac{U}{4}\hat{\sigma}_1^z + V\hat{\sigma}_2^z$. In this case the state of the first qubit does not affect the energy, reflecting the fact that there are always two degenerate states, one with $+\frac{1}{2}$ spin z projection, and one with $-\frac{1}{2}$ spin z projection. The 2 qubit circuit required to prepare any possible eigenstate of this Hamiltonian is shown in Fig. 2c, and consists of only one rotation. For two electrons there are two degenerate high-spin states, and the spin 0 singlet state, for which the Hamiltonian mapped to 2 qubits is $\hat{H} = \frac{U}{4}\hat{\sigma}_1^z\hat{\sigma}_2^z + V(\hat{\sigma}_1^z + \hat{\sigma}_2^z)$. The general 2-qubit ansatz for an eigenstate of this Hamiltonian is shown in Fig. 2b. Note that the CR approach is generally preferable over the PT approach, since it requires fewer angles as optimization parameters, and hence fewer gates and fewer qubits. The drawback is that it requires a mapping of the Hamiltonian to a reduced set of qubits with the desired number of electrons, which is a challenging task for a general Hamiltonian.

One important advantage of the chosen system is that it has exact analytical solutions, which we can therefore use to benchmark the quality of the quantum computations. The analytic DMFT solution for V is $V = \sqrt{z} = \sqrt{1 - \left(\frac{U}{6}\right)^2}$ for $U < 6$, and $V = \sqrt{z} = 0$ for $U \geq 6$, with $N_0 = 2$ and the singlet as GS. As first benchmarking test of the quantum algorithm we use a value of $U = 4$ and the corresponding analytic DMFT solution $V = 0.745356$, and compute the quantities needed to obtain $\omega_{p,n}$ and $\lambda_{p,\alpha,n}$. For convenience we now order the states in such a way that when they are degenerate, the smaller n refers to the spin up state, and the

TABLE I. Results of simulations on a classical computer without noise, comparing exact analytical results with those on a simulator for 4 qubits using the PT approach and for 2 qubits using the CR approach, for $U = 4$ and $V = 0.745356$. The parameters for the “Optimal θ ” sets were calculated with VQE using the ProjectQ simulator with infinite shots. These were then used as the parameters for the real devices runs on these sets. VQE optimized values for the angles θ .

	Exact	4 qubits			2 qubits		
		VQE (Infinite Shots)	VQE (10000 Shots)	Optimal θ (5000 Shots)	VQE (Infinite Shots)	VQE (10000 Shots)	Optimal θ (5000 Shots)
E_0	-1.795	-1.795	-1.801	-1.804	-1.795	-1.808	-1.811
$E_{3,0}$	-1.247	-1.247	-1.245	-1.232	-1.247	-1.254	-1.279
$E_{3,1}$	1.247	1.247	1.246	1.260	1.247	1.241	1.244
λ	0.2624	0.2624	0.2449	0.2877	0.2624	0.242	0.2734

TABLE II. Experimental data obtained on the IBM superconducting qubit quantum computer: the results correspond to those obtained by classical simulation in Table I. The “Optimal θ ” results have been measured using the angles optimized with the simulator, while for the data in the “VQE” columns the VQE optimization loop has been performed on the IBM device.

	Exact	4 qubits		2 qubits	
		Optimal θ (raw result)	Optimal θ (SPAM-cor.)	Optimal θ (SPAM-cor.)	VQE (SPAM-cor.)
E_0	-1.795	-1.196	-1.500	-1.700	-1.76
$E_{3,0}$	-1.247	-0.810	-1.111	-1.259	-1.29
$E_{3,1}$	1.247	1.001	1.025	1.253	1.29
λ	0.2624	0.1448	0.1128	0.2100	0.2477

larger n to the spin down state. Since the Hamiltonian is spin-symmetric, for $N = 3$ electrons we have 2 doubly degenerate independent energy eigenvalues ($E_{3,0} = E_{3,1}$ and $E_{3,2} = E_{3,3}$), where one is a spin up and the other one a spin down state. The poles in the GF (Eq. 7) are then found at $\omega_1 = \omega_{p,1,1} = \omega_{p,3,1} = E_{3,0} - E_0$ and $\omega_2 = \omega_{p,1,3} = \omega_{p,3,3} = E_{3,1} - E_0$, as well as at $-\omega_1$ and $-\omega_2$ due to ph symmetry. Furthermore we have $\lambda_{p,1,2} = \lambda_{p,1,4} = 0$, since these involve matrix elements between states with different spin. Since the GS has spin 0, $\lambda_{p,1,n}$ can be at most $1/2$. We therefore have only one independent parameter, and can write $\lambda_{p,1,1} = \lambda$ and $\lambda_{p,1,3} = 1/2 - \lambda$. For spin orbital 2 (spin down on site 1) the relations are analogous. To solve the DMFT problem we therefore need to calculate the two energies $E_{3,0}$ and $E_{3,2}$, and the single parameter λ on the quantum computer.

We first compute the GS using VQE with simulations of the algorithm on a classical computer, and for both the PT and the CR approaches we find that the GS is the singlet with $N_0 = 2$, in agreement with the analytical result. The values of E_0 for for the quantum simulation with effectively infinite statistical measurements are identical to the exact analytical results, and the same is true for $E_{3,0}, E_{3,1}$ and λ (see Table I), showing that our ansatz circuits can fully represent the eigenstates. For this simulation we use the actual wave function of the system, which effectively corresponds to the information obtained after an infinite amount of measurements. Any deviation from the exact results on a quantum device can therefore be attributed to the finite number of measurements (“shots”) and noise in the quantum computer. When we perform the VQE simulations for 10000 shots

per VQE step, the obtained energies are within about 2% of the exact numbers, while for λ the deviation is up to about 10%. We can also fix the angles θ in the circuit to the optimal values obtained with the VQE calculations for an effectively infinite number of shots, and perform a single step calculation with a finite number of shots at these “Optimal θ ” values. For 10000 shots the results are similar to those obtained using VQE with 10000 shots. If we reduce the number of shots to 5000, the discrepancies in the energy are still within about 2%, and for λ they are also still about 10%.

We can now perform the full DMFT loop simulation using the quantum circuit. Importantly, we need to regularize the calculated λ to satisfy the sum rule constraints discussed in Sec. II C, which in this case simplify to

$$\lambda = \frac{\omega_1^2 (V^2 - \omega_2^2)}{2V^2 (\omega_1^2 - \omega_2^2)}. \quad (22)$$

When applying regularization in the DMFT loop we therefore do not need to calculate λ on the quantum computer, since it is obtained with this relation. In this case we only need to obtain ω_1 and ω_2 via total energy calculations on the quantum computer. We find that in this way the DMFT loop with the quantum algorithm converges well for all U , and is only limited by statistical noise, while without regularization convergence cannot usually be achieved (Fig. 3). This is due to the appearance of unphysical divergences in the self-energy when Eq. (22) is not exactly fulfilled, as discussed in Sec. II C, which the regularization removes. The calculated values of z at DMFT self-consistency, z_{DMFT} , agree well with the exact analytical ones for all values of U (Fig. 3b). The only minor difference is that the transition from finite to zero

TABLE III. Experimental data obtained on the ion trap quantum computer at the University of Maryland: the results correspond to those obtained by classical simulation in Table I. The “Optimal θ ” results have been measured using the angles optimized with the simulator. The number in brackets gives the statistical error on the least significant digit.

	Exact	4 qubits		2 qubits	
		Optimal θ (raw result)	Optimal θ (SPAM-cor.)	Optimal θ (raw result)	Optimal θ (SPAM-cor.)
E_0	-1.795	-1.572(9)	-1.664(9)	-1.675(9)	-1.742(9)
$E_{3,0}$	-1.247	-1.039(8)	-1.111(8)	-1.165(6)	-1.208(6)
$E_{3,1}$	1.247	1.11(1)	1.122(9)	1.232(7)	1.230(7)
λ	0.2624			0.264(5)	0.258(5)

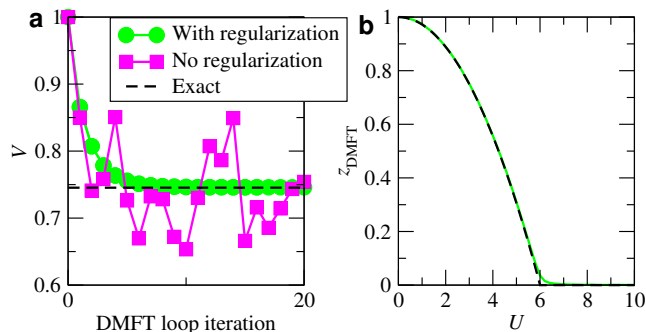


FIG. 3. a) Classical simulation of the DMFT algorithm for the change of the bath parameter V as function of DMFT loop iteration for a fixed value of $U = 4$, where 10000 shots are used for each simulated measurement. Using the regularization procedure to calculate λ (Eq. (22)) the bath parameter V converges quickly and smoothly to the correct value, while without regularization no convergence is possible. b) Value of the quasi-particle weight z at DMFT self-consistency, where $z = V^2$. The exact analytical value agrees well with the numerical result obtained using the quantum simulation.

z is somewhat smoothed out in the simulated results.

C. Experiments on quantum computers

To demonstrate that the algorithm runs successfully on current quantum computers we perform the calculation for the pair $U = 4$ and $V = 0.745356$ on two independent types of quantum computing hardware, the IBM superconducting qubit architecture (Table II) and the ion trap quantum computer at the University of Maryland (Table III). We use the quantum chemistry package EUMEN by Cambridge Quantum Computing (CQC) in combination with the `t|ket` compiler for circuit optimization, which is freely available to researchers⁵². To partly compensate for noise in the quantum hardware we apply standard corrections to the outputs for state preparation and measurement (SPAM) errors⁵³.

We run the experiments on superconducting qubits on the IBM Melbourne(QX4) quantum computer for the 4(2) qubit runs, and use 4096(8192) shots for a measurement. We use the SPAM library in CQC’s `t|ket` compiler for the 2 qubit measurements⁵⁴, and the equivalent

Qiskit’s Ignis library for the 4 qubit measurements⁵⁵.

The ion trap quantum computer at the University of Maryland is based on a chain of individual $^{171}\text{Yb}^+$ ions confined in a Paul trap^{56,57}. The native operations of the system are single qubit rotations, or R gates, and two-qubit entangling interactions, or XX gates, which are created by coupling any pair of qubits via the motional modes in the trap⁵⁸. This experiment is performed on a chain of seven ions, of which five are used as qubits. For the 4(2) qubit runs we use 4000(5000) shots per measurement. SPAM errors on the output distribution are corrected via the inverse of an independently measured state-to-state error matrix. This error characterization scales linearly with system size.

We first perform a measurement for fixed circuit parameter values set equal to the ones optimized on the classical simulator with VQE (Table I), using both the 4 qubit PT approach and the 2 qubit CR approach. The 4 qubit experiments on the IBM device give energies that are within about 35% of the exact values. When we correct for SPAM errors the results improve significantly and get to within about 10-20% of the exact values. For the 2 qubit CR experiments we obtain SPAM-corrected energies within about 5% of the exact ones, while for λ the deviation is larger, about 6%(50%) from the exact values for using the CR(PT) method. This larger error is expected, since the circuit to evaluate λ is longer than the one for the energies. Importantly, for a DMFT calculation λ is obtained from the exact sum rule (Eq. 22), so that the accuracy of the final result is entirely determined by the accuracy of the energies. On the ion trap device, the measurement outcomes are closer to the exact values. The SPAM corrected results on 4(2) qubits for the energy are within about 7-10%(1-3%) of the exact results, and λ for the CR method matches the exact value within the statistical uncertainty (Table III). The SPAM-correction has a smaller impact on these values since the measurement errors are lower than on the IBM device.

These results show that the required energies can be calculated rather accurately with experiments on the considered quantum devices. They also confirm that the CR approach generally gives results that are more noise-resilient. We therefore apply the CR method to perform a full VQE loop on a quantum computer. For this experiment we use the IBM QX4 device, and perform the

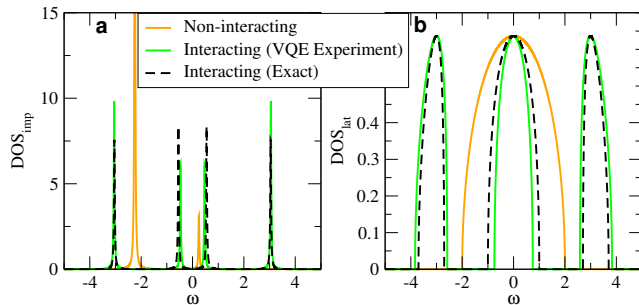


FIG. 4. (a) DOS on the impurity site and (b) corresponding DMFT DOS on the Bethe lattice for $U = 4$ and $V = 0.745356$, computed with many-electron interactions as a VQE experiment using the 2 qubit reduced circuit approach on the IBM quantum computer (green curve). The results of the experiment compare well with the exact analytical values (dashed curve). For comparison we also present the DOS without many-electron interactions (orange curve).

VQE optimization with the scikit-quantum implicit filtering stochastic minimizer⁵⁹. The VQE results in Tab. II show that it converges to within 3.5% of the exact results. The value of λ is accurate to 5.6%. These results are better than those obtained at the theoretical optimal angles on the same device, and are therefore indicative that the VQE loop partly compensates the calibration errors in the hardware.

Note that here in order to reduce the runtime of the experiments we have only presented VQE results at DMFT self-consistency. The experimental time for a full DMFT loop is the product of the single VQE loop time, and the number of iterations in the outer DMFT loop (Fig. 1). Given the high accuracy of the VQE results we expect that a full DMFT loop will exhibit similar convergence as the simulated one, and therefore reach self-consistency at about 10-20 iterations (Fig. 3a).

With the output of the VQE optimization at DMFT self-consistency one can then determine the electronic structure of the system. Using the energies calculated with VQE, and λ regularized using Eq. (22), we plot the DOS on the impurity site and on the corresponding Bethe lattice (Fig. 4). The agreement with the exact results is rather good, the small deviations are caused by the small differences in the energies of the VQE experiment and the exact analytical values. For reference we also present the

DOS obtained for the non-interacting system, which for the Bethe lattice has only a single broad peak, and therefore lacks the three peak structure of the DMFT result.

IV. CONCLUSIONS

We have presented an algorithm that performs DMFT calculations on currently available quantum computers. Our benchmarks on superconducting and trapped ion qubits for 2-site DMFT show that such practical calculations are possible with low levels of error. The reason is that the method is based on VQE total energy calculations, which are generally more resilient to noise than the real time evolution of states. The method will extend to growing system sizes compatible with near term quantum devices, and will benefit from the development for VQE calculations for quantum chemistry calculations of molecules, since the required quantum circuits are similar. We expect that our proof of concept demonstration that DMFT can be run on current quantum hardware will spark additional research into quantum algorithms for condensed matter physics systems.

V. ACKNOWLEDGMENTS

IR acknowledges financial support from the UK Department of Business, Energy and Industrial Strategy (BEIS). IR/RD/DR/NF acknowledge financial support from Innovate UK through the Analysis for Innovators Scheme A4I R3 Mini Project 104936. HC acknowledges the support through a Teaching Fellowship from UCL, LW acknowledges kindly the support through the Google PhD Fellowship in Quantum Computing. CHA acknowledges financial support from CONACYT (doctoral grant no. 455378). NML acknowledges financial support from the NSF Physics Frontier Center at JQI (grant no. PHY-1430094). EG is supported by the UK EPSRC [EP/P510270/1]. AP is supported by the InQUBATE Training and Skills Hub grant EPSRC EP/P510270/1. AP and IR thank the members of the EPSRC (grant No. 550520) Prosperity Partnership in Quantum Software for Modeling and Simulation for useful discussions.

* ivan.rungger@npl.co.uk

¹ S. J. Y. Macalino, V. Gosu, S. Hong, and S. Choi, Role of computer-aided drug design in modern drug discovery, *Archives of pharmacal research* **38**, 1686 (2015).

² J. Åqvist, C. Medina, and J.-E. Samuelsson, A new method for predicting binding affinity in computer-aided drug design, *Protein Engineering, Design and Selection* **7**, 385 (1994).

³ R. G. Parr, Density functional theory of atoms and molecules, in *Horizons of Quantum Chemistry* (Springer, 1980) pp. 5–15.

⁴ A. Jain, Y. Shin, and K. A. Persson, *Nature Rev. Mat.* **1**, 15004 (2016).

⁵ A. J. Cohen, P. Mori-Sánchez, and W. Yang, Insights into current limitations of density functional theory, *Science* **321**, 792 (2008).

- ⁶ M. Imada, A. Fujimori, and Y. Tokura, Metal-insulator transitions, *Reviews of modern physics* **70**, 1039 (1998).
- ⁷ C. Weber, D. D. O'Regan, N. D. Hine, P. B. Littlewood, G. Kotliar, and M. C. Payne, Importance of many-body effects in the kernel of hemoglobin for ligand binding, *Physical review letters* **110**, 106402 (2013).
- ⁸ C. Weber, D. J. Cole, D. D. O'Regan, and M. C. Payne, Renormalization of myoglobin–ligand binding energetics by quantum many-body effects, *Proceedings of the National Academy of Sciences* **111**, 5790 (2014).
- ⁹ N. Mardirossian and M. Head-Gordon, Thirty years of density functional theory in computational chemistry: an overview and extensive assessment of 200 density functionals, *Molecular Physics* **115**, 2315 (2017), <https://doi.org/10.1080/00268976.2017.1333644>.
- ¹⁰ J. Heyd, G. E. Scuseria, and M. Ernzerhof, Hybrid functionals based on a screened coulomb potential, *The Journal of Chemical Physics* **118**, 8207 (2003), <https://doi.org/10.1063/1.1564060>.
- ¹¹ A. Pertsova, C. M. Canali, M. R. Pederson, I. Rungger, and S. Sanvito, *Advances in Atomic, Molecular and Optical Physics* **64**, 29 (2015).
- ¹² F. Caruso, P. Rinke, X. Ren, A. Rubio, and M. Scheffler, Self-consistent *gw*: All-electron implementation with localized basis functions, *Phys. Rev. B* **88**, 075105 (2013).
- ¹³ W. Metzner and D. Vollhardt, Correlated lattice fermions in $d = \infty$ dimensions, *Phys. Rev. Lett.* **62**, 324 (1989).
- ¹⁴ A. Georges, G. Kotliar, W. Krauth, and M. J. Rozenberg, Dynamical mean-field theory of strongly correlated fermion systems and the limit of infinite dimensions, *Rev. Mod. Phys.* **68**, 13 (1996).
- ¹⁵ G. Kotliar and D. Vollhardt, Strongly correlated materials: Insights from dynamical mean-field theory, *Phys. Today* **57**, 53 (2004).
- ¹⁶ J. G. Bednorz and K. A. Müller, Possible high T_c superconductivity in the Ba-La-Cu-O system, *Zeitschrift für Physik B Condensed Matter* **64**, 189 (1986).
- ¹⁷ A. Droghetti and I. Rungger, Quantum transport simulation scheme including strong correlations and its application to organic radicals adsorbed on gold, *Phys. Rev. B* **95**, 085131 (2017).
- ¹⁸ E. G. Kovaleva and J. D. Lipscomb, Versatility of biological non-heme Fe(II) centers in oxygen activation reactions, *Nature chemical biology* **4**, 186 (2008).
- ¹⁹ V. Gesheva, S. Chausheva, N. Mihaylova, I. Manoylov, L. Dumanova, K. Idakieva, and A. Tchorbanov, Anticancer properties of gastropodan hemocyanins in murine model of colon carcinoma, *BMC immunology* **15**, 34 (2014).
- ²⁰ S. Lloyd, Universal quantum simulators, *Science* , 1073 (1996).
- ²¹ A. Aspuru-Guzik, A. D. Dutoi, P. J. Love, and M. Head-Gordon, Simulated quantum computation of molecular energies, *Science* **309**, 1704 (2005).
- ²² B. P. Lanyon, J. D. Whitfield, G. G. Gillett, M. E. Goggin, M. P. Almeida, I. Kassal, J. D. Biamonte, M. Mohseni, B. J. Powell, M. Barbieri, *et al.*, Towards quantum chemistry on a quantum computer, *Nature chemistry* **2**, 106 (2010).
- ²³ A. Y. Kitaev, Quantum measurements and the abelian stabilizer problem, 1995, arXiv preprint quant-ph/9511026 (1995).
- ²⁴ J. Preskill, Quantum computing in the NISQ era and beyond, *Quantum* **2**, 79 (2018).
- ²⁵ A. Peruzzo, J. McClean, P. Shadbolt, M.-H. Yung, X.-Q. Zhou, P. J. Love, A. Aspuru-Guzik, and J. L. O'Brien, A variational eigenvalue solver on a photonic quantum processor, *Nature Communications* **5**, 4213 (2014), ArXiv:1304.3061.
- ²⁶ A. Kandala, K. Temme, A. D. Córcoles, A. Mezzacapo, J. M. Chow, and J. M. Gambetta, Error mitigation extends the computational reach of a noisy quantum processor, *Nature* **567**, 491 (2019).
- ²⁷ J. D. Whitfield, J. Biamonte, and A. Aspuru-Guzik, Simulation of electronic structure hamiltonians using quantum computers, *Molecular Physics* **109**, 735 (2011).
- ²⁸ M. Benedetti, E. Lloyd, and S. Sack, Parameterized quantum circuits as machine learning models, arXiv preprint arXiv:1906.07682 (2019).
- ²⁹ M. Benedetti, E. Grant, L. Wossnig, and S. Severini, Adversarial quantum circuit learning for pure state approximation, *New Journal of Physics* **21**, 043023 (2019).
- ³⁰ K. Mitarai, M. Negoro, M. Kitagawa, and K. Fujii, Quantum circuit learning, *Physical Review A* **98**, 032309 (2018).
- ³¹ H. Chen, L. Wossnig, S. Severini, H. Neven, and M. Mohseni, Universal discriminative quantum neural networks, arXiv preprint arXiv:1805.08654 (2018).
- ³² X. Xu, J. Sun, S. Endo, Y. Li, S. C. Benjamin, and X. Yuan, Variational algorithms for linear algebra, arXiv preprint arXiv:1909.03898 (2019).
- ³³ B. Bauer, D. Wecker, A. J. Millis, M. B. Hastings, and M. Troyer, Hybrid quantum-classical approach to correlated materials, *Physical Review X* **6**, 1 (2016).
- ³⁴ D. Wecker, M. B. Hastings, N. Wiebe, B. K. Clark, C. Nayak, and M. Troyer, Solving strongly correlated electron models on a quantum computer, *Physical Review A* **92**, 062318 (2015).
- ³⁵ J. M. Kreula, L. García-Álvarez, L. Lamata, S. R. Clark, E. Solano, and D. Jaksch, Few-qubit quantum-classical simulation of strongly correlated lattice fermions, *EPJ Quantum Technology* **3**, 1 (2016).
- ³⁶ M. Potthoff, Two-site dynamical mean-field theory, *Physical Review B - Condensed Matter and Materials Physics* **64**, 1 (2001).
- ³⁷ M. Caffarel and W. Krauth, Exact diagonalization approach to correlated fermions in infinite dimensions: Mott transition and superconductivity, *Physical Review Letters* **72**, 1545 (1994).
- ³⁸ S. Qimiao, J. Rozenberg, G. Kotliar, and A. E. Ruckenstein, expression, *Physical Review Letters* **72**, 2761 (1994).
- ³⁹ A. Liebsch and H. Ishida, Temperature and bath size in exact diagonalization dynamical mean field theory, *Journal of Physics Condensed Matter* **24**, 10.1088/0953-8984/24/5/053201 (2012).
- ⁴⁰ D. Wecker, B. Bauer, B. K. Clark, M. B. Hastings, and M. Troyer, Gate-count estimates for performing quantum chemistry on small quantum computers, *Physical Review A* **90**, 022305 (2014).
- ⁴¹ W. J. Huggins, J. McClean, N. Rubin, Z. Jiang, N. Wiebe, K. B. Whaley, and R. Babbush, Efficient and noise resilient measurements for quantum chemistry on near-term quantum computers, arXiv preprint arXiv:1907.13117 (2019).
- ⁴² E. Fradkin, Jordan-wigner transformation for quantum-spin systems in two dimensions and fractional statistics, *Phys. Rev. Lett.* **63**, 322 (1989).
- ⁴³ C. A. Perroni, H. Ishida, and A. Liebsch, Exact diagonalization dynamical mean-field theory for multiband materi-

- als: Effect of coulomb correlations on the fermi surface of $\text{na}_{0.3}\text{coo}_2$, Phys. Rev. B **75**, 045125 (2007).
- ⁴⁴ K. Temme, S. Bravyi, and J. M. Gambetta, Error mitigation for short-depth quantum circuits, Phys. Rev. Lett. **119**, 180509 (2017).
- ⁴⁵ Y. Li and S. C. Benjamin, Efficient variational quantum simulator incorporating active error minimization, Phys. Rev. X **7**, 021050 (2017).
- ⁴⁶ Suguru Endo, I. Kurata, and Y. O. Nakagawa, Calculation of the green's function on near term quantum computer, arXiv:arXiv:1909.12250v1.
- ⁴⁷ K. T. M. T. M. B. J. M. C. Abhinav Kandala, Antonio Mezzacapo and J. M. Gambetta, Hardware-efficient variational quantum eigensolver for small molecules and quantum magnets, Nature **549**, 242 (2017).
- ⁴⁸ I. G. Ryabinkin, S. N. Genin, and A. F. Izmaylov, Constrained variational quantum eigensolver: Quantum computer search engine in the fock space, Journal of Chemical Theory and Computation **15**, 249 (2019).
- ⁴⁹ leonardoguidoni (GitHub), Modifying hamiltonian and wave function for vqe in quantum chemistry issue 37 qiskit-community/qiskit-camp-europe-19, accessed: 2019-10-07.
- ⁵⁰ K. M. Nakanishi, K. Mitarai, and K. Fujii, Subspace-search variational quantum eigensolver for excited states (2018), arXiv:1810.09434.
- ⁵¹ O. Higgott, D. Wang, and S. Brierley, Variational Quantum Computation of Excited States, Quantum **3**, 156 (2019).
- ⁵² <https://cqcl.github.io/pytket/build/html/index.html>, [t|ket) repository].
- ⁵³ Yunseong Nam, Ground-state energy estimation of the water molecule on a trapped ion quantum computer, arXiv:arXiv:1902.10171v2.
- ⁵⁴ A. Cowtan, S. Dilkes, R. Duncan, A. Krajenbrink, W. Simons, and S. Sivarajah, On the Qubit Routing Problem, in *14th Conference on the Theory of Quantum Computation, Communication and Cryptography (TQC 2019)*, Leibniz International Proceedings in Informatics (LIPIcs), Vol. 135, edited by W. van Dam and L. Mancinska (Schloss Dagstuhl–Leibniz-Zentrum fuer Informatik, Dagstuhl, Germany, 2019) pp. 5:1–5:32.
- ⁵⁵ H. A. et al., Qiskit: An open-source framework for quantum computing (2019).
- ⁵⁶ S. Debnath, N. M. Linke, C. Figgatt, K. A. Landsman, K. Wright, and C. Monroe, Demonstration of a small programmable quantum computer with atomic qubits, Nature **536**, 63 (2016).
- ⁵⁷ K. A. Landsman, C. Figgatt, T. Schuster, N. M. Linke, B. Yoshida, N. Y. Yao, and C. Monroe, Verified quantum information scrambling, Nature **567**, 61 (2019).
- ⁵⁸ T. Choi, S. Debnath, T. A. Manning, C. Figgatt, Z.-X. Gong, L.-M. Duan, and C. Monroe, Optimal quantum control of multimode couplings between trapped ion qubits for scalable entanglement, Phys. Rev. Lett. **112**, 190502 (2014).
- ⁵⁹ scikit-quant (GitHub), Imfil scikit quant stochastic minimizer, accessed: 2019-10-07.